2026 IEEE/SICE International Symposium on System Integration (SII)
January 11-14, 2026. Cancún, México

Pass-On Control: Personalized Assistive Online Control for a Wrist Exosuit

Jacob Behrendt*,1 and Marc-Anton Scheidl*,1 and Sabine Thuerauf[1] and Claudio Castellini[1,2]

***Abstract*— We present a multimodal control system for a tendon-driven soft wrist exosuit that delivers personalized, angle- and mode-sensitive assistance during wrist flexion-extension. Our hierarchical architecture combines surface electromyography (sEMG) and inertial measurements through a three-layer controller comprising an intent recognizer, an angle-specific EMG normalization layer, and a low-level impedance controller. In a pilot study with four healthy participants performing repetitive wrist tasks at slow and fast speeds, with and without a 2.5 kg load, our controller substantially compensated the additional external load when present. Compared with unassisted trials under load, median normalized extensor activity decreased by approximately 30% (Cohen's $d > 1.7$), and the fatigue-related drift in EMG across repetitions was eliminated. In contrast, assistance slightly increased EMG in the no-load condition. Assistance introduced a modest accuracy penalty: root-mean-square error and peak error rose by roughly $1-2^\circ$ but remained below 4° on average. These results demonstrate that integrating angle-dependent EMG normalization with inertial sensing enables effective, task-specific unloading of the wrist while maintaining functional accuracy. Our findings lay the groundwork for larger studies and clinical applications of soft wrist exosuits.**

I. Introduction

Wearable robotic exoskeletons are increasingly used for assistive and rehabilitative purposes to enhance motor function in individuals with impairments and to augment the capabilities of healthy users (e.g., overhead tasks in industry) [1]. However, the rigid structures of exoskeletons suffer from various problems. Individual joint alignment requires significant time and is essential for proper function. However, most models are heavy and uncomfortable, limiting usability over extended periods [2], [3]. Additionally, many exoskeletons show a lack of portability and tend to remain in rehabilitation labs. Only a few passive models, mainly for industrial use, are seen outside such controlled environments [2]. In contrast, soft exosuits are a lightweight solution that offer inherent compliance and improved comfort [1], [2]. Their soft materials and tendon-driven transmissions bypass joint misalignment entirely [2].

Impairment of wrist function (e.g., post-stroke hemiparesis or radial-nerve injury) can severely limit hand use [4], [5]. Assistive wrist exoskeletons can provide additional force to the impaired joints. They can improve the ability of users with muscle weakness to perform activities of daily living. Yet, they remain under-prescribed due to shortcomings in current device designs and control strategies [6]. A common approach to scale output force according to the user's intent is proportional myoelectric control (PMC), which scales assistive torque to the user's surface electromyography (sEMG) signals [7]. Linear PMC has been applied in elbow and wrist devices [7], [8], but these simple mappings are limited in robustness across postures and over time [8]. In particular, sEMG amplitude varies substantially with joint angle due to biomechanical factors. To date, few controllers have performed real-time angle normalization of sEMG. Advanced techniques (e.g., Hill-type muscle models or machine-learning regressors) exist to model the sEMG–torque relationship more accurately, but they demand extensive calibration and computation [9], [10]. These gaps highlight the need for more adaptive, control architectures tailored to wrist biomechanics and user intent [11], [12].

To address these challenges, we introduce a multimodal control system that integrates sEMG and inertial measurement units (IMUs) for sensing, along with a hierarchical control architecture. Our approach dynamically compensates for load based on sEMG signals and joint angles, utilizing IMU-based angle estimation for calibrated polynomial mappings. To improve within-range consistency of assistance, we compensate for joint-angle–dependent sEMG amplitude using angle-specific normalization, which reduces posture sensitivity relative to fixed-gain proportional myoelectric mappings [7], [8], [13], [14], while avoiding the calibration and computational burden of musculoskeletal model–based approaches [10]. This simple model ensures a quick computation that runs in real-time. High-level intent recognition classifies the user's activity (extension or flexion), and the system dynamically engages tailored modes, with specific assistive strategies. By combining real-time multimodal sensing with a three-layer control architecture (high-level intent recognition, mid-level assistive control, and low-level impedance control), the exosuit provides compliant assistance in real time. In summary, this paper presents the design and integration of a simple, multimodal control system for a tendon-driven wrist exosuit, without a musculoskeletal model, and evaluates its effectiveness through a pilot user study.

II. Methods

This section describes the hardware and sensing platform of the wrist exosuit, the angle-specific sEMG normalization procedure, the hierarchical control architecture, and the design of the pilot user study.

[1]Jacob Behrendt, Marc-Anton Scheidl, Sabine Thuerauf and Claudio Castellini are with the Assistive Intelligent Robotics Lab, Friedrich-Alexander-Universität Erlangen-Nürnberg, 91052 Erlangen, Germany marc.scheidl@fau.de

[2]Claudio Castellini is also with the Institute of Robotics and Mechatronics, German Aerospace Centre, 82234 Oberpfaffenhofen, Germany

*These authors contributed equally to this work.

A. Exosuit Hardware and Sensors

The assistive device is a soft wrist exosuit that actuates flexion-extension through two brushless DC motors (AK60-6 motors, CubeMars, Nanchang, China) [15] driving a pair of tendons (woven DuPont Aramid fiber, 90 kg traction). The motors are mounted on a lightweight testbed, and the tendons are routed along custom guides towards a wristband that integrates an IMU and across to a soft glove. This setup enables the 9 Nm peak output torque of the motors to produce a torque of approximately 20 Nm at the wrist joint. The glove follows prior exosuit designs that route tendons along the palmar and dorsal surfaces of the hand [16], [17]. Instead of a dedicated in-line load cell, due to the additional bulk, tendon tension is monitored via the built-in torque estimator of the MD80 motor driver (MAB Robotics, Poznań, Poland) and used to enforce safety limits in a closed-loop control architecture [18].

Two MYO (Thalmic Labs, Kitchener, Canada) armbands provide eight sEMG channels each, sampled at 200 Hz. The raw sEMG signal is amplified, high-pass filtered at 10 Hz, rectified, and then low-pass filtered by a second-order Butterworth filter with a 4 Hz cut-off to extract the envelope (mean absolute value, ARV). Because the relevant envelope frequencies are below 25 Hz, the 16-dimensional envelope feature is down-sampled to 50 Hz to reduce computational load. Mathematically, the sEMG pre-processing adds a $\approx$ 112 ms delay. Simultaneously, two custom-built IMUs (Model: BNO08X, Bosch, Germany) deliver quaternion-based 3D orientation at 200 Hz [19]. Both sensors stream their raw data to a host machine, where the signal is pre-processed, classified, and used for torque prediction using our custom C#-framework [20], [21]. At the same time, a Raspberry Pi (Sony UK Technology Centre, Wales, UK) performs low-level actuation and communicates motor commands over a Controller Area Network (CAN) bus [22], [23]. A photo of the assembled wrist-exosuit mounted in the testbed is provided in Figure 1.

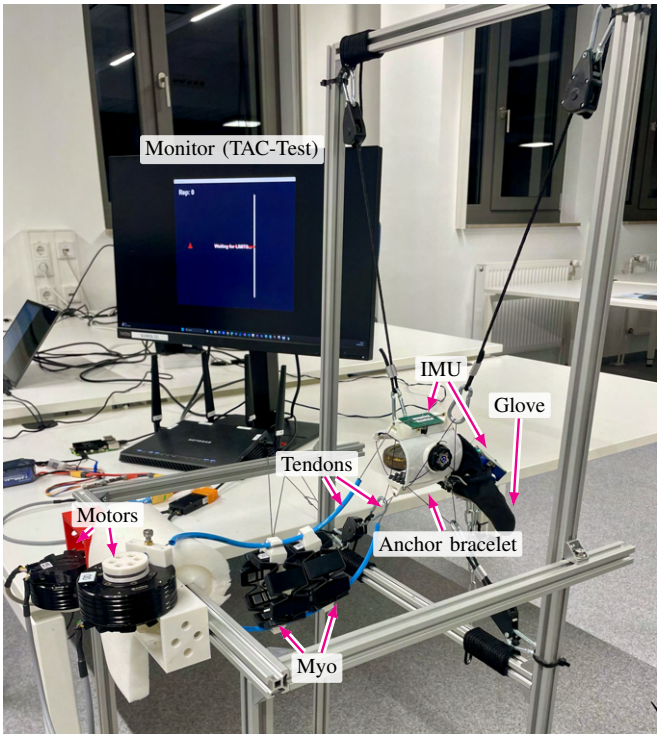

Fig. 1: Prototype tendon-driven wrist exosuit. Motors with tendon routing are mounted on a forearm anchor brace; tendons attach to a glove to apply flexion/extension torques. Monitor with the target achievement (TAC) test nearby. Sensorization via sEMG and IMU.

B. Angle-Specific sEMG Normalization

During an individual calibration session, participants perform maximal voluntary contractions (MVCs) "at five equally spaced joint angles within the participant's ROM in both extension and flexion. The resulting peak ARV values are recorded and fitted with third-order polynomials for each movement direction, allowing for the smooth and quick compensation of sEMG-angle non-linearities without the risk of over-parameterization [14]. Prior work indicates that polynomial sEMG–angle normalization is effective for lower limb joints [13].

$$sEMG_{max}(\theta) = k_0 + k_1\theta + k_2\theta^2 + k_3\theta^3 \qquad (1)$$

where $sEMG_{max}(\theta) \in \mathbb{R}$ is the expected maximum sEMG envelope for a specific angle, $\theta \in \mathbb{R}$ is the specific exosuit angle, and k_0, k_1, k_2, and $k_3 \in \mathbb{R}$ are the coefficients of the fitted polynomial. The fitted polynomials are sampled every 1° to produce lookup tables that map joint angle to the expected maximum sEMG envelope, thus drastically enhancing the performance during runtime. At runtime, the current sEMG envelope $ARV(t, \theta) \in \mathbb{R}$ is divided by the angle-specific maximum to yield a normalized activation value $a(\theta) \in [0, 1]$.

$$a(\theta) = \frac{ARV(t, \theta)}{sEMG_{max}(\theta)} \qquad (2)$$

This angle-aware normalization compensates for posture-dependent variations in sEMG amplitude and ensures that subsequent torque commands reflect the user's effort rather than joint position.

C. Control Architecture

The exosuit employs a three-layer hierarchical control architecture (Figure 2), comprising a high-level intent recognition module, a mid-level assistive policy generator, and a low-level impedance controller. Processed sEMG and IMU signals are streamed to the high- and mid-level controllers via Bluetooth Low Energy and 5 GHz local Wi-Fi, respectively, with negligible transmission delay. The low-level controller executes on the embedded motor driver at 40 kHz, with inner velocity and outer position loops operating at 5 kHz and 1 kHz, respectively.

1) High-Level Classification: In this work, *intention* is defined operationally as the user's *current* assistive request (i.e., desired wrist movement class: *rest*, *extension*, or *flexion*). To enable high-level control prediction, the normalized sEMG envelopes from 16 channels are arranged into a feature vector, which is passed to an incremental ridge regression classifier trained during calibration. This model outputs continuous scores for the movement classes $i \in \{rest, extension, flexion\}$; a softmax function then converts these scores into probabilities p_i. A class is activated only if its probability exceeds a minimum threshold and is higher than the second-largest probability by at least $\Delta P \in \mathbb{R}$; otherwise, the system remains in the rest state. This gating introduces hysteresis and avoids switching when class probabilities are close [24], [25], [26]. In our experiment, we use $p_{min} \approx 0.3$ and $\Delta P \approx 0.10$ during the ≈ 1 min calibration and kept them fixed per participant.

2) Nonlinear sEMG-to-Torque Mapping: The mid-level controller computes the desired assistive torque $\omega(a) \in \mathbb{R}$ based on the normalized activation $a(\theta)$ and the classified intent as shown in Eq. 3. The torque *sign* is set by the active mode from the high-level controls, while Eq. 3 provides the magnitude. The assistance adapts continuously only through the angle-normalized activation $a(\theta)$. Below a relative activation threshold $a_{\min} \in \mathbb{R}$, a constant preload torque $\omega_{\min} \in \mathbb{R}$ maintains cable tension. For activations above $a_{\min}$, the desired torque obeys a logistic function

$$\omega(a(\theta)) = \omega_{\max} \cdot \frac{1}{1 + \exp\big[-k(a(\theta) - a_c)\big]}, \qquad (3)$$

where $\omega_{\max} \in \mathbb{R}$ sets the maximum assistive torque, $a_c \in \mathbb{R}$ positions the sigmoid centre, and $k \in \mathbb{R}$ defines its slope. Adjusting $(a_{\min}, a_c, \omega_{\min}, \omega_{\max})$ allows the response to be tuned to individual preferences. In the pilot, direction-specific defaults were used: extension ($\omega_{\max} = 6\,\mathrm{Nm}$, $\omega_{\min} = 0.3\,\mathrm{Nm}$), flexion ($\omega_{\max} = 7\,\mathrm{Nm}$, $\omega_{\min} = 0.5\,\mathrm{Nm}$); $a_c = 0.5$ and $k = 3$ in both directions. Activation floors were $a_{\min,\mathrm{ext}} = 0.18$ and $a_{\min,\mathrm{flex}} = 0.20$. A baseline cable-tension floor of $0.2\,\mathrm{Nm}$ was maintained at rest.

3) Low-Level Impedance Control: The low-level controller on the MD80 driver emulates a virtual spring–damper at a reference angle and enforces the resulting torque via impedance control:

$$\tau = k_P\,(\theta_{\mathrm{ref}} - \theta) + k_D\,(\dot{\theta}_{\mathrm{ref}} - \dot{\theta}) + \tau_{\mathrm{ff}}, \qquad (4)$$

with

$$\tau, \theta, \theta_{\mathrm{ref}}, \dot{\theta}, \dot{\theta}_{\mathrm{ref}}, \tau_{\mathrm{ff}} \in \mathbb{R}, \quad k_P, k_D \in \mathbb{R}_{>0}.$$

where $k_P\,(\theta)$ is the stiffness and $k_D\,(\dot{\theta})$ the damping. $(\theta_{\mathrm{ref}} = 0, \dot{\theta}_{\mathrm{ref}} = 0)$ are the reference position and velocity from the mid-level impedance controller, and $\tau_{\mathrm{ff}} = \omega(a)$ is the desired assistive torque feed-forward term [27]. The driver continuously monitors motor current, encoder feedback, and internal torque estimates to maintain safe tendon tension and disable assistance if thresholds are exceeded [18].

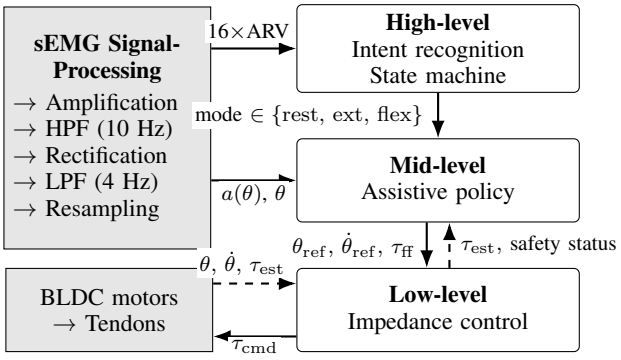

Fig. 2: Three-layer control architecture with explicit mode gating and angle-aware sEMG normalization. Processed sEMG feeds a high-level intent recognizer and a mid-level policy that computes time-varying torque magnitude $\omega(a)$. The low-level impedance controller enforces the commanded torque (Eq. 4). Dashed lines are feedback signals and solid lines are commands.

D. Controller Calibration

Each participant undergoes a calibration procedure to personalize the sEMG normalization and intent classifier. First, the user performs MVCs for extension and flexion at 5, within the participant's range of motion (ROM), equally distributed joint angles; the system records peak ARV values and fits third-order polynomials as described in Section II-B. These lookup tables are later used to normalize sEMG envelopes to percentage MVC, assuming that the sEMG-angle relationship is smooth and cubic [13]. Second, the high-level classifier is trained: the user is instructed to rest, extend, and flex the wrist while ARV features are collected, yielding three seconds of data per class. An incremental ridge regression algorithm is fitted to these data and used to recognize intention in real time [24], [25]. Notably, the whole calibration procedure took approximately 1 minute. After calibration, users practice a few assisted movements to familiarize themselves with the device.

E. Participants and Experimental Design

Four healthy adults (three male, one female; mean age 26.3 ± 3.6 years) with no history of upper-limb disorders participated after providing written consent. A within-subject factorial design manipulated Assistance (On/Off), Load (0 kg vs. 2.5 kg), Speed (45°/s vs. 90°/s), and Movement Direction (extension vs. flexion), resulting in $2 \times 2 \times 2 \times 2 = 16$ conditions presented in a counterbalanced order.

Participants performed wrist movements in a pronated forearm position with the hand oriented horizontally, such that wrist extension was performed against gravity and wrist flexion was performed with gravity. In the 0 kg condition, the load corresponded to the weight of the hand acting through gravity. In the 2.5 kg condition, an additional 2.5 kg mass was attached to the hand, increasing the gravitational torque during extension and reducing it during flexion.

Each trial comprised 20 repetitions of a wrist motion, starting from neutral and alternating between maximal extension

and flexion at the prescribed speed. Participants followed a continuous target trajectory displayed on a screen and were instructed to keep the wrist angle indicator aligned with the target. The repetition was successful when the target end position was reached. Five-minute breaks were inserted between runs to minimize fatigue. The user performed all calibrations and practice trials before the experimental runs.

F. Outcome Measures

Muscle activation was quantified as the median ARV (normalized to the angle-specific MVC) of the extensor muscle channels per repetition, averaged within each condition. sEMG variance and the rate of change of ARV across repetitions served as proxies for muscle fatigue [28]. Tracking accuracy was evaluated by the root-mean-square error (RMSE) between the actual and target wrist angle and by the peak absolute error per repetition. Shapiro-Wilk tests verified normality of the dependent variables ($p > 0.05$). A repeated-measures Analysis of Variance (rmANOVA) (with factors Assistance, Load, Speed, and Direction) was conducted, followed by Holm-Bonferroni-corrected paired t-tests where appropriate. Significance thresholds were set at $\alpha = 0.05$.

III. Results

The results are divided into three sections. Firstly, the changes in total sEMG amplitude represent the muscle activation. Secondly, the observations regarding fatigue are presented. Finally, the third section shows the kinematic tracking accuracy.

A. Median averaged rectified sEMG amplitude

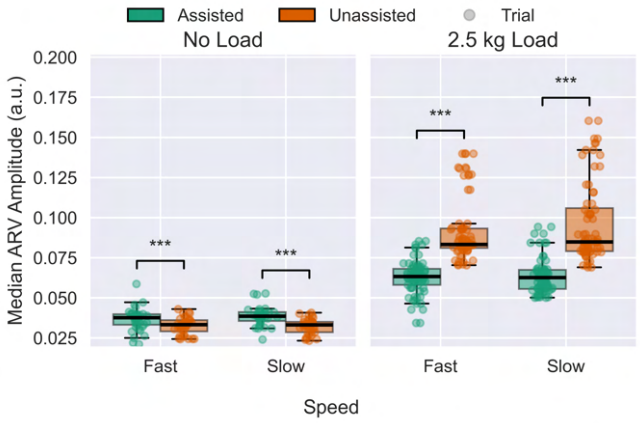

Fig. 3: Median ARV amplitude during wrist extension. Cyan = assisted, orange = unassisted. Left: no load; right: 2.5 kg load; each panel shows fast vs. slow tracking. Horizontal brackets mark significant paired contrasts.

The ARV of the extensor muscles served as the primary effort metric. rmANOVA revealed that the external load had a substantial main effect ($F(1,3) = 184.2$, $p < 0.001$). A significant *Assistance* × *Load* interaction was observed ($F(1,3) = 48.8$, $p < 0.01$), indicating that assistance influences sEMG amplitude differently depending on whether a weight is present.

Without an external load, assistance increased the median ARV by $\approx 18\%$. The effect sizes were negative in extension ($d = -0.6$) and flexion ($d = -0.3$). Conversely, when lifting the 2.5 kg weight, assistance markedly reduced sEMG amplitude. The reductions were large for the extension (Cohen's $d = 1.8$ in the fast condition, $d = 1.7$ in the slow condition) and moderate-to-large for flexion ($d = 0.7$-1.0). Averaged across all speeds, the assisted trials showed roughly a 30% decrease in median ARV activity relative to unassisted trials under 2.5 kg load. In contrast, the no-load condition exhibited a slight increase in effort with assistance in place. These results demonstrate that the exosuit's unloading effect manifests primarily when an external torque challenges the wrist.

B. Fatigue-related sEMG ARV drift

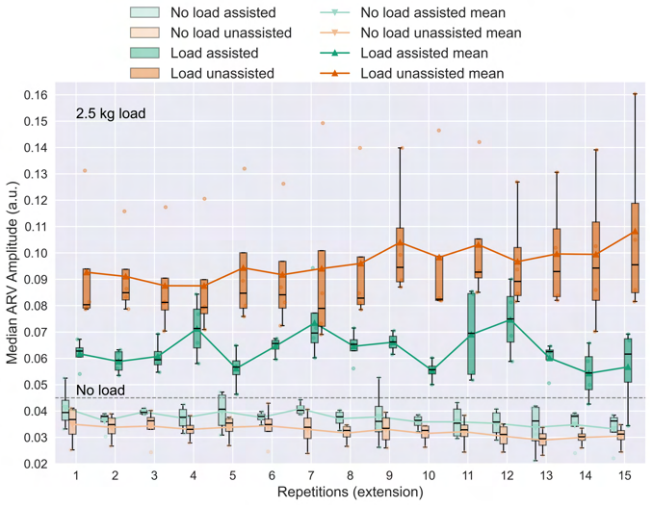

Fig. 4: Median ARV per repetition under 2.5 kg load (top) and no-load (bottom). Loaded assisted ARV change over time remains flat; unassisted ARV rises.

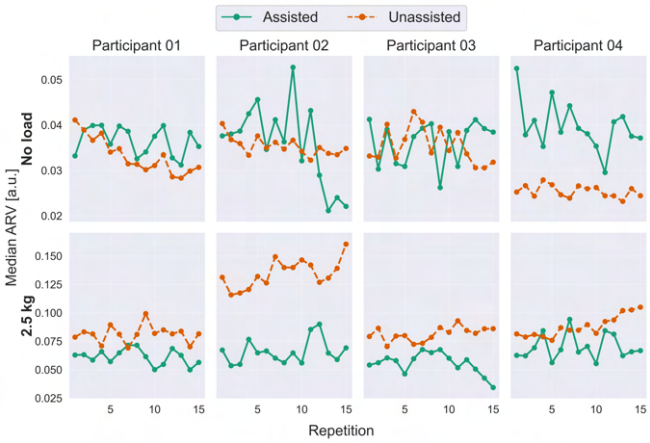

Fig. 5: Median ARV per repetition under 2.5 kg load and no-load per participant.

To examine fatigue, we analyzed the evolution of median ARV over successive repetitions. Each run consisted of 20

full flexion-extension cycles. To ensure steady-state conditions of the sEMG envelopes and movement execution, we excluded the first three and last two flexion–extension cycles. Initial cycles often contain motor-adaptation transients (e.g., familiarization with the device), whereas final cycles exhibit attention-related variability and task-termination effects. The remaining 15 cycles provide a stable core segment for the slope analysis, allowing for consistent subdivision into early, middle, and late task phases for the fatigue analysis. Under the 2.5 kg load, the unassisted median ARV increased linearly across repetitions (slope $\beta = +0.0024$ a.u./rep, $p < 0.001$), whereas the assisted series showed no significant drift (Fig. 4). An early-late comparison confirmed that unassisted sEMG rose significantly from 0.082 a.u. to 0.093 a.u. ($t = -11.406$, $p < 0.0005$, $d = 5.16$). In contrast, the assisted condition exhibited no significant change ($t = -0.890$, $p = 0.424$, $d = 0.48$). Participant-wise inspection (Fig. 5) confirms that this upward drift in the unassisted loaded condition occurred consistently across all participants, with particularly pronounced increases in Participants 02–04. These findings indicate that the exosuit mitigated fatigue-related increases in muscle activation when the wrist was loaded, without causing additional fatigue in the no–load condition, as indicated by Figure 4. Without load, the assisted and unassisted ARV activity shows no drift and remains flat at a low baseline across all repetitions.

C. Kinematic tracking accuracy

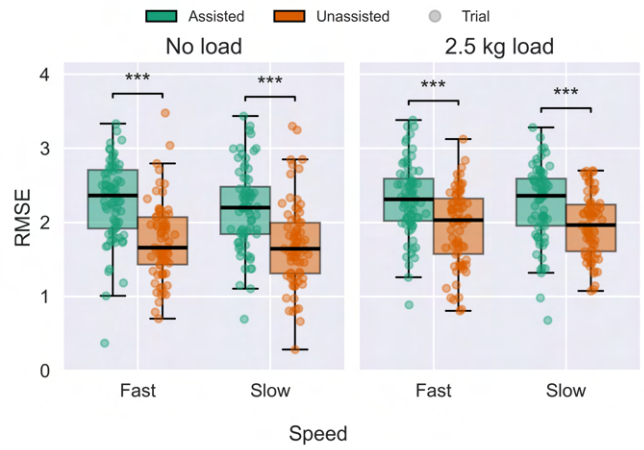

Fig. 6: Wrist-angle tracking RMSE by load and speed for flexion and extension. Each box plots the distribution of per-segment RMSE values (z-standardized within participants).

Kinematic accuracy was assessed using the RMSE and peak error between the target trajectory and the measured wrist angle. Errors were computed for each repetition, then standardized within participants. Across conditions, assistance increased tracking error relative to unassisted trials: the rmANOVA on z-standardized RMSE showed a near-significant main effect of condition ($F(1,3) = 9.271$, $p = 0.056$) and a significant *Condition* × *Load* interaction ($F(1,3) = 10.482$, $p < 0.05$). Absolute RMSE values nevertheless remained below 4° on average, and peak errors also rose modestly with assistance; a separate rmANOVA on peak error yielded a significant main effect of condition ($F(1,3) = 11.435$, $p < 0.05$). There were no significant interactions involving speed or movement direction (all $p > 0.05$), indicating that the accuracy penalty was invariant across these factors.

IV. Discussion

This work investigated a multi-modal, angle- and mode-sensitive control system for a soft-wrist exosuit. The controller combines angle-specific sEMG normalization and inertial sensing with a three-layer architecture that applies torque assistance. A pilot study involving four healthy participants assessed the impact of this system on muscle activation and kinematic accuracy during repetitive wrist tasks with and without an external load.

A. Effort reduction and fatigue mitigation

Consistent with our hypothesis, the exosuit markedly reduced extensor muscle activity when participants lifted a 2.5 kg mass. Under load, median sEMG amplitudes decreased by roughly 30% relative to unassisted trials, with large effect sizes in extension and moderate-to-large effects in flexion. Importantly, this unloading effect was contingent on the presence of external torque; without load, the median ARV tended to be slightly increased, and effect sizes were negative. Fatigue analysis further showed that, under load, unassisted sEMG drifted upward across repetitions, whereas assisted sEMG remained flat, indicating that the controller mitigates neuromuscular fatigue when the musculature is challenged. However, in the no-load case, the slopes of both conditions showed similarly small gradients. These results demonstrate that angle-specific sEMG normalization coupled with a logistic torque mapping can provide meaningful assistance without inducing fatigue. Still, they also underscore the task-specific nature of the benefits: assistance is most useful during loaded movements and may be counter-productive during no-load tasks.

B. Accuracy trade-offs and mechanical considerations

The principal drawback observed was a modest but systematic increase in tracking error when assistance was provided. The RMSE and peak error were higher in the assisted condition across load and speed combinations. Although z-standardized RMSE exhibited a near-significant main effect of condition and a significant interaction with load, absolute RMSE values remained below 4° on average and thus within functional bounds. Notably, this magnitude is comparable to the intrinsic dynamic orientation error of the BNO080 inertial sensor used for angle tracking, whose typical dynamic rotation error is approximately 3.5° and static error 2.0° according to the manufacturer's specification [19]. Hence, the observed deviation approaches the sensor's inherent accuracy limit rather than representing a substantial degradation of kinematic performance. The increase in error likely stems from mechanical compliance inherent in the tendon-driven

prototype: slack in the glove and forearm brace introduces a delay between commanded and delivered torque, leading to overshoot and oscillations, particularly when no external load is present. Similar effort-accuracy trade-offs have been reported for other upper-body exoskeletons [29]. Mitigating this penalty will require hardware refinements (stiffer tendon routing, adjustable braces, decoupled sensor mounts) and control-level adaptations (tuning impedance gains and adopting torque mappings that account for dynamic coupling).

C. Limitations and future work

This pilot study involved four participants and served primarily to demonstrate feasibility. Accordingly, rmANOVA results should be interpreted descriptively, with emphasis on effect sizes rather than p-values. Larger and more diverse cohorts, including stroke survivors and older adults, are needed to draw robust conclusions about therapeutic efficacy and usability. The MYO armbands operated at 200 Hz, which was adequate for envelope extraction but precluded spectral fatigue analyses. Future implementations should employ higher-resolution sEMG systems ($\geq 1\,\mathrm{kHz}$) to enable frequency-domain metrics. Additionally, adhesive electrodes may reduce potential electrode shift, increasing signal robustness further. The sEMG envelope pipeline adds ≈ 112 ms; with negligible transmission, the end-to-end delay is ≈ 120 ms. This falls within typical real-time budgets ($<$ 300 ms) for myoelectric control [30], [31], [32], [33], [34]. A slight cable preload was maintained to suppress slack-induced transients and maintain instant force transmission. The controller relied on cubic polynomial sEMG-angle maps and a fixed logistic model to convert normalized sEMG into assistive torque. While these mappings are computationally efficient [10], they may not capture individual biomechanical nuances. Furthermore, we did not benchmark them against a musculoskeletal model-based PMC. Our claim is conceptual: angle-specific sEMG normalization aims to improve within-ROM consistency compared to fixed-gain control [7], [8], [13], [14]. While the on-board torque estimator provided sufficient, yet unspecified bandwidth for safe operation in this prototype, a more advanced exosuit revision would benefit from compact in-line load cells, which would enable more accurate tendon-force sensing and allow baseline tendon preload to be reduced below the ≈ 0.2 Nm floor imposed here by the estimator accuracy. Future work could explore denser calibration protocols or adaptive neuromechanical models that update online. Finally, movement-intent classification used a simple ridge regression trained on a few seconds of data; more sophisticated classifiers (e.g., support vector machines or lightweight neural networks) may improve robustness and generalizability [24], [25].

Overall, this study demonstrates the feasibility of integrating angle-normalized sEMG and inertial sensing in a hierarchical control scheme for a wrist exosuit. The controller provides substantial unloading and fatigue mitigation during loaded tasks, while incurring a minor penalty in kinematic accuracy. These findings lay the groundwork for future clinical evaluations and motivate continued refinement of both hardware and control strategies.

V. Conclusion

This study demonstrates the feasibility of integrating angle-normalized sEMG and inertial sensing within a hierarchical control framework for a soft-wrist exosuit. By combining a high-level intent detection and classification with angle-specific sEMG normalization and a nonlinear torque mapping, the controller delivers angle- and mode-sensitive assistance that adapts to user effort and joint posture. Active assistance from the exosuit markedly reduced muscular effort and mitigated fatigue when the wrist operated against a 2.5 kg load. Kinematic accuracy declined modestly with assistance, yet absolute tracking errors remained within measurable limits. These findings highlight a fundamental trade-off between unloading and precision, underscoring the importance of tailoring assistance to the task and user.

Given the small sample size and simplified hardware, the present results should be interpreted as proof of concept. Future work should explore mechanical refinements to reduce compliance and latency, integrate higher-fidelity sEMG sensors and more robust intent classifiers, and evaluate the system in larger and clinically diverse cohorts. Ultimately, such improvements could enable soft exosuits to transition from laboratory prototypes to versatile assistive devices that augment hand and wrist function in daily life.

ACKNOWLEDGMENT

This work was (partially) supported by the German Federal Ministry of Education and Research (BMBF) under the Robotics Institute Germany (RIG).

References

[1] E. Bardi, M. Gandolla, F. Braghin, F. Resta, A. L. G. Pedrocchi, and E. Ambrosini, "Upper limb soft robotic wearable devices: a systematic review," *Journal of NeuroEngineering and Rehabilitation*, vol. 19, no. 1, p. 87, Aug. 2022. [Online]. Available: https://jneuroengrehab.biomedcentral.com/articles/10.1186/s12984-022-01065-9

[2] M. Xiloyannis, R. Alicea, A.-M. Georgarakis, F. L. Haufe, P. Wolf, L. Masia, and R. Riener, "Soft robotic suits: State of the art, core technologies and open challenges," *IEEE Transactions on Robotics*, vol. 38, no. 3, pp. 1343–1362, Jun. 2022, arXiv:2105.10588 [cs]. [Online]. Available: http://arxiv.org/abs/2105.10588

[3] R. F. Pitzalis, D. Park, D. G. Caldwell, G. Berselli, and J. Ortiz, "State of the Art in Wearable Wrist Exoskeletons Part I: Background Needs and Design Requirements," *Machines*, vol. 11, no. 4, p. 458, Apr. 2023. [Online]. Available: https://www.mdpi.com/2075-1702/11/4/458

[4] L. A. Simpson and J. J. Eng, "Functional Recovery Following Stroke: Capturing Changes in Upper-Extremity Function," *Neurorehabilitation and Neural Repair*, vol. 27, no. 3, pp. 240–250, Mar. 2013. [Online]. Available: https://pubmed.ncbi.nlm.nih.gov/23077144/

[5] W. Z. Ray and S. E. Mackinnon, "Clinical Outcomes Following Median to Radial Nerve Transfers," *The Journal of Hand Surgery*, vol. 36, no. 2, pp. 201–208, Feb. 2011. [Online]. Available: https://linkinghub.elsevier.com/retrieve/pii/S0363502310011901

[6] A. Galbert and A. Buis, "Active, actuated, and assistive: a scoping review of exoskeletons for the hands and wrists," *Canadian Prosthetics and Orthotics Journal*, vol. 7, no. 1, p. 43827, 2024. [Online]. Available: https://pmc.ncbi.nlm.nih.gov/articles/PMC11609922/

[7] T. Lenzi, S. M. M. De Rossi, N. Vitiello, and M. C. Carrozza, "Proportional EMG control for upper-limb powered exoskeletons," in *2011 Annual International Conference of the IEEE Engineering in Medicine and Biology Society*. Boston, MA: IEEE, Aug. 2011, pp. 628–631. [Online]. Available: https://pubmed.ncbi.nlm.nih.gov/22254387/

[8] Z. Tang, K. Zhang, S. Sun, Z. Gao, L. Zhang, and Z. Yang, "An Upper-Limb Power-Assist Exoskeleton Using Proportional Myoelectric Control," *Sensors*, vol. 14, no. 4, pp. 6677–6694, Apr. 2014. [Online]. Available: https://www.mdpi.com/1424-8220/14/4/6677

[9] Q. Wu, B. Chen, and H. Wu, "Neural-network-enhanced torque estimation control of a soft wearable exoskeleton for elbow assistance," *Mechatronics*, vol. 63, p. 102279, Nov. 2019. [Online]. Available: https://linkinghub.elsevier.com/retrieve/pii/S0957415819301126

[10] N. Lotti, M. Xiloyannis, G. Durandau, E. Galofaro, V. Sanguineti, L. Masia, and M. Sartori, "Adaptive Model-Based Myoelectric Control for a Soft Wearable Arm Exosuit: A New Generation of Wearable Robot Control," *IEEE Robotics & Automation Magazine*, vol. 27, no. 1, pp. 43–53, Mar. 2020. [Online]. Available: https://ieeexplore.ieee.org/document/8963852/

[11] A. M. Abdullahi, A. Haruna, and R. Chaichaowarat, "Hybrid Adaptive Impedance and Admittance Control Based on the Sensorless Estimation of Interaction Joint Torque for Exoskeletons: A Case Study of an Upper Limb Rehabilitation Robot," *Journal of Sensor and Actuator Networks*, vol. 13, no. 2, p. 24, Mar. 2024. [Online]. Available: https://www.mdpi.com/2224-2708/13/2/24

[12] N. Karavas, A. Ajoudani, N. Tsagarakis, J. Saglia, A. Bicchi, and D. Caldwell, "Tele-impedance based assistive control for a compliant knee exoskeleton," *Robotics and Autonomous Systems*, vol. 73, pp. 78–90, Nov. 2015. [Online]. Available: https://linkinghub.elsevier.com/retrieve/pii/S0921889014002127

[13] J. E. Earp, R. U. Newton, P. Cormie, and A. J. Blazevich, "Knee angle-specific EMG normalization: The use of polynomial based EMG-angle relationships," *Journal of Electromyography and Kinesiology*, vol. 23, no. 1, pp. 238–244, Feb. 2013. [Online]. Available: https://linkinghub.elsevier.com/retrieve/pii/S1050641112001514

[14] M. Behrens, F. Husmann, A. Mau-Moeller, J. Schlegel, E.-M. Reuter, and V. R. Zschorlich, "Neuromuscular Properties of the Human Wrist Flexors as a Function of the Wrist Joint Angle," *Frontiers in Bioengineering and Biotechnology*, vol. 7, p. 181, Aug. 2019. [Online]. Available: https://pubmed.ncbi.nlm.nih.gov/31497595/

[15] CubeMars, "Ak60-6 v1.1 kv80," 2025, accessed on: 25.07.2025. [Online]. Available: https://www.cubemars.com/product/ak60-6-v1-1-kv80-robotic-actuator.html

[16] D. Chiaradia, L. Tiseni, M. Xiloyannis, M. Solazzi, L. Masia, and A. Frisoli, "An Assistive Soft Wrist Exosuit for Flexion Movements With an Ergonomic Reinforced Glove," *Frontiers in Robotics and AI*, vol. 7, p. 595862, Jan. 2021. [Online]. Available: https://www.frontiersin.org/articles/10.3389/frobt.2020.595862/full

[17] C. Lambelet, M. Lyu, D. Woolley, R. Gassert, and N. Wenderoth, "The eWrist — A wearable wrist exoskeleton with sEMG-based force control for stroke rehabilitation," in *2017 International Conference on Rehabilitation Robotics (ICORR)*. London: IEEE, Jul. 2017, pp. 726–733. [Online]. Available: https://ieeexplore.ieee.org/document/8009334/

[18] MAB Robotics, *MD80 v3.0 motor controller*, 2025, accessed on: 25.07.2025. [Online]. Available: https://www.mabrobotics.pl/product-page/md80-motor-controller

[19] Hillcrest Laboratories, Inc., *BNO080: 9-Axis Smart Sensor System in Package (SiP) with Integrated Sensor Fusion*, revision 1.3 ed., Hillcrest Laboratories, Inc., Rockville, MD, USA, October 2017, datasheet. [Online]. Available: https://www.ceva-ip.com/wp-content/uploads/BNO080_085-Datasheet.pdf

[20] P. Visconti, F. Gaetani, G. Zappatore, and P. Primiceri, "Technical Features and Functionalities of Myo Armband: An Overview on Related Literature and Advanced Applications of Myoelectric Armbands Mainly Focused on Arm Prostheses," *International Journal on Smart Sensing and Intelligent Systems*, vol. 11, no. 1, pp. 1–25, Jan. 2018. [Online]. Available: https://sciendo.com/article/10.21307/ijssis-2018-005

[21] M. Connan, M. Sierotowicz, B. Henze, O. Porges, A. Albu-Schäffer, M. A. Roa, and C. Castellini, "Learning to teleoperate an upper-limb assistive humanoid robot for bimanual daily-living tasks," *Biomedical Physics & Engineering Express*, vol. 8, no. 1, p. 015022, Jan. 2022. [Online]. Available: https://iopscience.iop.org/article/10.1088/2057-1976/ac3881

[22] Raspberry Pi Foundation, "Raspberry Pi 5," 2024, accessed on: 25.07.2025. [Online]. Available: https://www.raspberrypi.com/products/raspberry-pi-5/

[23] MAB Robotics, "Candle," 2023, accessed on: 25.07.2025. [Online]. Available: https://www.mabrobotics.pl/product-page/candle

[24] A. Phinyomark, A. Nuidod, P. Phukpattaranont, and C. Limsakul, "Feature Extraction and Reduction of Wavelet Transform Coefficients for EMG Pattern Classification," *Elektronika ir Elektrotechnika*, vol. 122, no. 6, pp. 27–32, Jun. 2012, number: 6. [Online]. Available: https://eejournal.ktu.lt/index.php/elt/article/view/1816

[25] D. P. Losey, C. G. McDonald, E. Battaglia, and M. K. O'Malley, "A Review of Intent Detection, Arbitration, and Communication Aspects of Shared Control for Physical Human–Robot Interaction," *Applied Mechanics Reviews*, vol. 70, no. 1, p. 010804, Jan. 2018. [Online]. Available: https://asmedigitalcollection.asme.org/appliedmechanicsreviews/article/70/1/010804/443697/A-Review-of-Intent-Detection-Arbitration-and

[26] A. Fougner, Øyvind, P. J. Kyberd, Y. G. Losier, and P. A. Parker, "Control of Upper Limb Prostheses: Terminology and Proportional Myoelectric Control—A Review," *IEEE Transactions on Neural Systems and Rehabilitation Engineering*, vol. 20, no. 5, pp. 663–677, Sep. 2012. [Online]. Available: https://ieeexplore.ieee.org/document/6205630/

[27] N. Hogan, "Impedance Control: An Approach to Manipulation: Part I—Theory," *Journal of Dynamic Systems, Measurement, and Control*, vol. 107, no. 1, pp. 1–7, Mar. 1985. [Online]. Available: https://asmedigitalcollection.asme.org/dynamicsystems/article-abstract/107/1/1/400604/Impedance-Control-An-Approach-to-Manipulation-Part?redirectedFrom=fulltext

[28] M. Xiloyannis, D. Chiaradia, A. Frisoli, and L. Masia, "Physiological and kinematic effects of a soft exosuit on arm movements," *Journal of NeuroEngineering and Rehabilitation*, vol. 16, p. 29, Feb. 2019. [Online]. Available: https://www.ncbi.nlm.nih.gov/pmc/articles/PMC6385456/

[29] J. Gräf, S. Grospretre, A. Argubi-Wollesen, and B. Wollesen, "Impact of a passive upper-body exoskeleton on muscular activity and precision in overhead single and dual tasks: an explorative randomized crossover study," *Frontiers in Neurology*, vol. 15, p. 1405473, Jun. 2024. [Online]. Available: https://doi.org/10.3389/fneur.2024.1405473

[30] L. H. Smith, L. J. Hargrove, B. A. Lock, and T. A. Kuiken, "Determining the optimal window length for pattern recognition-based myoelectric control: balancing the competing effects of classification error and controller delay," *IEEE Transactions on Neural Systems and Rehabilitation Engineering*, vol. 19, no. 2, pp. 186–192, 2011.

[31] T. R. Farrell and R. F. Weir, "The optimal controller delay for myoelectric prostheses," *IEEE Transactions on Neural Systems and Rehabilitation Engineering*, vol. 15, no. 1, pp. 111–118, 2007.

[32] C. Igual, L. A. J. Pardo, J. M. Hahne, and J. Igual, "Myoelectric control for upper limb prostheses," *Electronics*, vol. 8, no. 11, p. 1244, 2019.

[33] S. Tam, M. Boukadoum, A. Campeau-Lecours, and B. Gosselin, "Intuitive real-time control strategy for high-density myoelectric hand prosthesis using deep and transfer learning," *Scientific Reports*, vol. 11, no. 1, p. 11275, 2021.

[34] C. Attig, N. Rauh, T. Franke, and J. F. Krems, "System latency guidelines then and now — is zero latency really considered necessary?" in *Engineering Psychology and Cognitive Ergonomics. EPCE 2017*, ser. Lecture Notes in Computer Science. Cham: Springer, 2017, vol. 10276, pp. 2–14.